Spectrometer for shot-to-shot photon energy characterization in the multi-bunch mode of the free electron laser at Hamburg

S. Palutke[1,2,a)], N. C. Gerken[1], K. Mertens[1], S. Klumpp[1], A. Mozzanica[3], B. Schmitt[3], C. Wunderer[2], H. Graafsma[2], K.-H- Meiwes-Broer[4], W. Wurth[1,2] and M. Martins[1]

[1]*University of Hamburg, Institute for Experimental Physics, Luruper Chaussee 149, D-22761 Hamburg, Germany*

[2]*Deutsches Elekronen Synchrotron (DESY), Notkestraße 85, D-22607 Hamburg, Germany*

[3]*Paul Scherrer Institute (PSI), Ch-5232 Villigen, Swiss*

[4]*University of Rostock, Institute for Physics, Universitätsplatz 3, D-18051 Rostock, Germany*

[a)] Author to whom correspondence should be addressed; electronic mail: steffen.palutke@desy.de

The setup and first results from commissioning of a fast online photon energy spectrometer for the vacuum ultraviolet free electron laser at Hamburg (FLASH) at DESY are presented. With the use of the latest advances in detector development the presented spectrometer reaches readout frequencies up to 1 MHz. In this paper we demonstrate the ability to record online photon energy spectra on a shot-to-shot base in the multi-bunch mode of FLASH. Clearly resolved shifts in the mean wavelength over the pulse train as well as shot-to-shot wavelength fluctuations arising from the statistical nature of the photon generating Self Amplified Spontaneous Emission (SASE) process have been observed. In addition to an online tool for beam calibration and photon diagnostics, the spectrometer enables the determination and selection of spectral data taken with a transparent experiment up front over the photon energy of every shot. This leads to higher spectral resolutions without the loss of efficiency or photon flux by using single-bunch mode or monochromators.

I. INTRODUCTION

Free electron lasers (FELs) have opened new areas in the field of photon-matter interaction. With their high peak brilliance and intensity they give access to new experiments focusing on the dynamics and the interaction of matter with intense radiation like nonlinear effects.[1-8] The first short wavelength FEL is the **F**ree Electron **Las**er **H**amburg (FLASH)[9-13] at DESY. With its 27 m undulator length in total it produces short, coherent, linearly polarized vacuum ultraviolet or soft x-ray radiation pulses with pulse durations of a few 10 fs between 4.2 nm and 45 nm[14] in the fundamental. It reaches peak intensities of 10^{13} photons per shot or pulse and brilliances of 10^{30} photons/(s mrad² mm² 0.1 % BW).[11] A unique property of FLASH and the upcoming European X-FEL[15] is the superconducting linear accelerator. It enables pulse rates larger than 1 kHz, which is at least one order of magnitude more than other existing FELs. At FLASH up to 800 electron bunches with a maximum bunch frequency of 1 MHz form a bunch train. The bunch trains are generated with a repetition frequency of 10 Hz. This is the designed bunch structure of FLASH and is called multi-bunch mode in contrast to the single-bunch mode, where a bunch train consists of only one bunch. Pulses with these high radiation values are generated by the so called **S**elf **A**mplifying **S**pontaneous

Emission (SASE) process.[12,16-19] It is of statistical nature and causes fluctuations in all photon beam properties like photon energy, intensity, spectral bandwidth, pulse duration and mode structure of the pulses.[20-23] For instance, the mean photon energy of the FLASH beam varies around 1 % to 2 % on average. For spectroscopic experiments this variation leads to reduced spectral resolution and, therefore, to a more difficult interpretation of the measured data, especially, when performing experiments with a low signal, which cannot generate a notable spectrum within a single pulse. For example, Senz et al.[24] and Bahn et al.[25] performed photoelectron spectroscopy on very dilute metal cluster beams in order to investigate their size-dependent electronic structure. Despite the high flux of the FEL, the low target density leads to low count rates and requires the integration or summation over many FEL shots. The photon energy fluctuations are included through this approach and limit the energy resolution of the spectra.

To enhance the resolution one has to use monochromators[26] or measure the photon energy simultaneously[27,28]. Until recently, there were no detectors available that met the requirements to measure photon energy spectra with readout frequencies of up to 1 MHz. By using available systems for online measurements one has to switch to single-bunch mode of FLASH with only one pulse per pulse train.[27,28] This option is often not desirable because the reduced total flux makes experiments at dilute targets inefficient or even impossible. However, the last advances and developments in detector technology have made the needed or even higher repetition rates possible.[29-31]

In this paper we present the setup and commissioning results of a spectrometer combined with a slightly modified version of the new **G**ain **O**ptimizing micros**T**rip sys**T**em wit**H** **A**nalog **R**ea**D**out (GOTTHARD) detector[30,31]. It is a result of a joint development of the Paul Scherrer Institute (PSI) and DESY and offers for the first time the capability of measuring photon energy spectra on a shot-to-shot base in the multi-bunch mode of FLASH, in other words, of every pulse of a pulse train.

II. SETUP

The aim was to build a grating based spectrometer with the capability to resolve the photon energy fluctuations of the FEL pulses with pulse frequencies of up to 1 MHz over the whole wavelength range provided by FLASH. Spectrometers based on photoelectron or ion spectroscopy of gas targets[32,33] fulfill the temporal requirements but their disadvantage is a dependence on the kind and pressure of the chosen target and on the photon beam intensity. Therefore, we decided to use a grating as dispersive element to overcome space charge and non-linear effects, which result in spectral distortions and prevent an easy or online photon energy analysis.

For single-shot detection of the dispersed distribution behind a grating, a detector is needed with sufficient multi-hit capability and spatial resolution. Most of the available detectors for direct photon detection like CCD's or ICCD's do not provide the required readout speed. 2D-Detectors with readout frequencies of 1 MHz or even more, such as the Adaptive Gain Integrating Pixel Detector (AGIPD)[34], are currently under development. The GOTTHARD detector[31] is a single line detector, already available and can provide readout frequencies up to 1 MHz with low noise and conservation of linear response.

A further requirement is a compact and mobile design to connect the spectrometer to different transparent experiments within the limited space given in the experimental hall of FLASH. With a grating as dispersive element the size limitation results in a small focal length and, therefore, in a limitation of lateral dispersion in the focal plane. To get a reasonable resolution which is sufficient to clearly resolve the fluctuations produced due to the SASE process, an indirect way of detection is chosen. A schematic sketch of the spectrometer setup is given in figure 1 and illustrates the underlying basic idea.

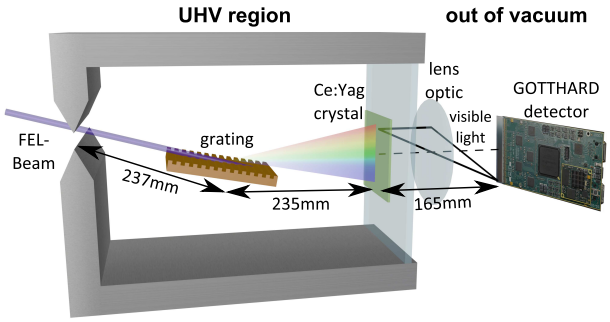

FIG. 1: (Color online) Schematic sketch of the function principle of the spectrometer. The dispersed XUV light from the FEL hits a Ce:YAG crystal located in the focal plane of the grating and generates a visible fluorescence. The position of the fluorescence on the crystal depends on the wavelength of the FEL beam and is imaged and magnified via an out of vacuum lens system onto the detector. The lengths given are the focal path lengths inside the spectrograph and the distance of the GOTTHARD sensor from the vacuum viewport.

The XUV light from the FEL is dispersed by a spherical grating. Depending on the wavelength of the incident photons the dispersed light hits different positions on a cerium-doped yttrium-aluminum garnet (Ce:YAG) crystal. The crystal fully absorbs the XUV light and generates fluorescence in the visible regime. The fluorescence is imaged and magnified via an out of vacuum lens system onto the sensitive area of the detector. The magnification compensates the small dispersion which results from the limitations given above. This design grants an access to the lens system and the detector without breaking the vacuum and has the advantage that the magnification and, therefore, the resolution of the whole spectrometer, are easily changeable even during measurements. A drawback of this setup is the reduction of the number of photons through the magnification and the optical elements.

In detail we use a modified 251MX UHV soft x-ray spectrograph from McPherson. The first modification is a welding of three additional flanges on the top flange. Two ports are aligned with the light path of the incoming non-dispersed beam. The front one is equipped with a manipulator that holds a plate with pin holes of different diameters, the rear is equipped with another Ce:YAG crystal. The third flange is a viewport directed at this crystal. Together with the entrance slit they allow a precise alignment of the chamber to the FEL beam. The second modification is a shortening of the exit port. In the standard design the port holds a CCD and the image focal plane of the grating falls onto the detection surface of the camera. For our purposes the exit port was shortened to be able to hold a vacuum chamber with a linear feedthrough. On the feedthrough the Ce:YAG crystal located in the image focal plane is mounted.

This compact spectrograph features two variable line spacing (VLS), concave, spherical, holographic replica gratings with a gold coating.[35-37] The two gratings are mounted at a fixed angle on holders attached to a rail system and are selectable under vacuum via a linear feedthrough. The gratings are aberration corrected for best resolution, have a nearly flat focal plane in their designed wavelength regions and have a laminar groove profile, which effectively suppresses higher orders and stray light[38]. The Low Energy Grating[35,36] (LEG) has a curvature radius of 5606 mm, an effective groove density of 1200 l/mm and is designed for wavelengths between 5 nm and 20 nm. The High Energy Grating[37] (HEG) with a curvature radius of 15920 mm and an effective groove density of 2400 l/mm covers the region between 1 nm and 6 nm. Nevertheless, both gratings are useable for even larger wavelengths. In our experiment the HEG is used at a wavelength of 12.3 nm. The thereby occurring deviation of the focal curve from the presumed plane is negligible and we have the advantage of a higher dispersion. With the information and the focal curves provided by the manufacturer it is possible to estimate the size of the spectral distribution. Assuming a 1 % fluctuation of the average wavelength of 12.3 nm the spectral distribution on the Ce:YAG screen measures approximately 400 µm when using the LEG and 600 µm when the HEG is used.

The FEL beam enters the spectrograph through an entrance slit. It is adjustable between 5 µm and 3 mm and was set to 150 µm during the experiment. The light travels a 237 mm long path through two apertures and impinges on the used HEG at an angle of 88.65°. The beam spot of the entrance slit plane is then imaged at the focal plane located 235 mm from the parallel grating normal.

The Ce:YAG crystal mounted in the focal plane of the gratings measures $10 \times 10 \times 0.1$ mm³ and can be moved along the dispersion axis with the linear feedthrough. A Ce doped YAG crystal can withstand the intense FEL radiation, has a small fluorescence decay constant of 70 ns and a fluorescence radiation mainly in the green-yellow optical regime between 500 nm and 650 nm. This is suitable to the needs to clearly distinguish the pulses with a separation of 1 µs at the highest possible frequency of 1 MHz and to transfer the light to the detector outside the vacuum. According to experiences with other spectrometers and monitors using Ce:YAG crystals for indirect beam detection[26,39,40], a crystal of such thickness does not show saturation effects at the expected photon flux or blurring, which could result in reduced energy resolution.

The magnifying lens system consists of two lenses measuring 9 mm in diameter. The first is an achromatic lens with an effective focal length of 12 mm. The distance from the lens surface to the Ce:YAG crystal is approximately 12.6 mm. Between the crystal and the lens a 6 mm quartz glass window with a multilayer anti-reflective coating for the fluorescence main wavelength of 550 nm separates the vacuum from the non-vacuum side. The second lens has a focal length of 9 mm and is located 68 mm behind the first one. The sensor surface of the GOTTHARD detector is approximately 75 mm away from the second lens. The lens system provides a total magnification of approximately 34. Assuming the 600 µm spectral distribution on the Ce:YAG screen by using the HEG, as mentioned above, the image has a diameter of around 20 mm on the sensor.

The GOTTHARD detector used in this experiment is presented by Mozzanica *et al.*[30,31] and will be summarized in the following. It is a 1D detector and has a 64×8 mm² microstrip silicon sensor with a 50 µm pitch resulting in a

single line of 1280 strips. As the GOTTHARD is developed to detect hard x-rays out of vacuum the strips are shielded from visible light by an aluminum coating. It provides single photon detection down to photon energies of 7 keV. The core elements of the detector are the ten implemented Application Specific Integrated Circuits (ASIC). Each of them contains a periphery circuitry for the digital control and the I/O functionality and has 128 identical, parallel operating channels. Each channel is wire bonded to a strip and has a preamplifier with charge integrating configuration in its front end block. The gain of the preamplifier has three selectable settings and is adjusted automatically by the front end circuit through continuous monitoring by a comparator. The fast readout speed of up to 1 Mhz is realized by a parallelization of the readout architecture to 4 analog outputs per ASIC chip. The 128 input channels of each chip are grouped into ensembles of 32. Every group is connected via a distributed multiplexer, which is clocked by a 32 MHz readout clock and connects one channel at a time to the chip's off driver. Besides the ASICs and the sensor, the basic board holds a Field Programmable Gate Array (FPGA), the control and readout electronics, Gbit and other I/O ports as well as an embedded Linux system. Together, this forms a compact and easy manageable GOTTHARD module.

For the experiment described here, the GOTTHARD had to be slightly modified. To detect the photons from the Ce:YAG crystal the sensor has to be sensitive to visible light. Therefore, the protective Al coating was removed by an etching process. The other changes are software related with regards to the implementation of the GOTTHARD module into the FLASH Data Acquisition (DAQ) system. For the use at the multi-bunch mode of FLASH with a 10 Hz bunch train repetition frequency and a bunch frequency of up to 1 MHz the detector has to be used in the so called "burst mode". In this mode a trigger starts the internal clock control of the GOTTHARD module. Opening time, repetition frequency and a defined number of single line images or frames are programmed via a Graphical User Interface (GUI) and controlled by the software of the GOTTHARD module itself. The single line images are cached in the FPGA during the pulse train and are extracted over the Gbit interface between two trigger events.

The lens system and the detector are mounted on an optical bench outside the vacuum chamber and their distances are easily adjustable during the measurements. An optically opaque fabric encased the exit port of the spectrograph, the lens system and the detector front side with the sensitive sensor area to prevent stray light. The spectrograph, the lens system and the detector are placed on an optical breadboard, which sits in a holding of a supporting frame. Screws fixing the breadboard allow a precise alignment in the horizontal directions and angle in relation to the beam. The frame contains wheels and height-adjustable pedestals. They provide beam heights between 1.35 m and 1.65 m and allow the connection to various beamlines. The moveable frame has a floor space of about $550 \times 760\ mm^2$. From the beamline port to the end of the rail holding detector and lenses the whole spectrometer has a length below one meter and fulfills the required compactness and flexibility.

For a reasonable use as a diagnostic tool or spectrometer for FLASH the GOTTHARD has to be fully implemented into the FLASH DAQ architecture. The taken data has to be synchronized with the data coming from other instruments, monitors and experiments at the beamline or the accelerator. In figure 2 a sketch of the beamline configuration with the mainly used instruments in the experiment is shown to illustrate the necessary implementations and alignments.

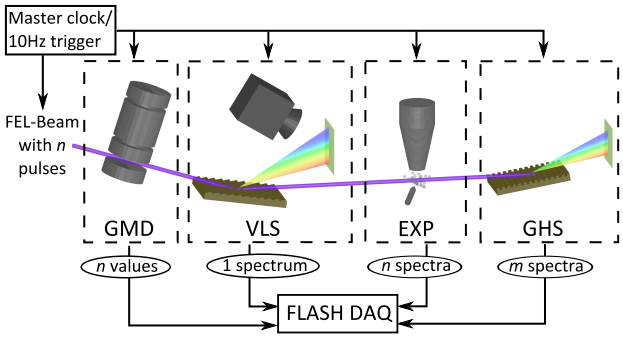

FIG. 2: (Color online) Beamline schematics for the performed experiment. Along the path of the FEL beam with *n* pulses per pulse train the main detectors and data sources are shown: The Gas Monitor Detector (GMD), the variable line spacing spectrometer (VLS), a transparent experiment (EXP) and the GOTTHARD spectrometer (GHS). In our case the experiment is a Time-of-Flight (ToF) photoelectron/photoion spectrometer for gaseous targets. The FEL beam generation and all data sources are triggered by the FLASH master clock. The kind and amount of data transferred to the DAQ per trigger event or per pulse train differs and is depicted in the ellipses. The DAQ generates a unique event-ID per trigger event and sorts the data by it.

The instruments used are the Gas Monitor Detector (GMD)[22,41], a variable line spacing grating spectrometer (VLS)[40], a transparent experiment (EXP) and the GOTTHARD spectrometer (GHS). In our case the transparent experiment was a photoelectron and photoion spectroscopy (PES/PIS) chamber for gaseous targets.[42]

The GMD is part of the beamline infrastructure of FLASH and located before the branching point to the different beamlines. A detailed description is given by Richter *et al.*[41] and Tiedtke *et al.*[22]. In short, it measures online the energy of every photon pulse of a pulse train. The beam ionizes a rare gas target whose ions and electrons are accelerated towards oppositely mounted electrodes by an electric field. The number of photons and the recorded energy of each pulse can be deduced from the measured electron and ion signal.

The VLS spectrometer is an online photon energy spectrometer, also implemented in the FLASH beamline and described in detail by Brenner *et al.*[40] In summary, the FEL beam impinges on one of two selectable variable line spacing blazed gratings at a fixed angle of 88°. About 1 % to 10 % of the incident radiation is dispersed for analysis, while the rest is reflected in the zeroth order towards the experimental section of the beamline. The first order diffraction is focused onto a Ce:YAG crystal located in the focal plane and produces a fluorescence. Its position holds the information about the photon energy and is imaged by a gated intensified CCD with 1280×1024 pixels and a pixel size of 7 µm. The camera and the crystal are mounted on a moveable detection unit and follow the focal curve for the whole wavelength range of the two gratings from 6 nm to 60 nm. Due to the use of a gated ICCD with a readout frequency of 10 Hz single-shot spectra of a specific pulse of a pulse train can be recorded and observed online. The VLS is mounted in the BL branch before the branching point to the three BL beamlines.

The PES/PIS experiment is an UHV chamber for gaseous targets and described in the thesis of N. Gerken[42]. Briefly, a diffusive beam of rare gases or vaporized liquids is supplied by a gas needle and crossed with the FEL beam. With high resolution Time-of-Flight spectrometers ion- and electron spectroscopy can be performed on a shot-to-shot basis.

All devices from FEL beam generation to data acquisition and storage are triggered by the FLASH master clock. For every trigger event the FLASH DAQ system provides all incoming data with a unique event-ID number and a time stamp. Therefore, correct triggering and synchronization of all data sources are crucial. The obstacle is the varying processing times of different data sources due to the varying amount of data and different processing steps. In figure 2 the amount of data per bunch train or per 10 Hz trigger event from the mainly used instruments is depicted. The ellipses show the data from every part of the experiment produced by one trigger event. The number *n* is the number of bunches within the bunch train. The GMD and the VLS generate a moderate amount of data with *n* values or one image per trigger event, respectively. The PES/PIS experiment generates as many spectra as bunches within the train and the number of spectra from the GOTTHARD spectrometer *m* can be changed and normally exceeds the number of bunches ($m>n$). The choice to take more frames than the number of bunches or pulses generated from FLASH was due to the fact, that we wanted to clearly observe the beginning and the end of the pulse train for verification and to get several frames without beam as background. The *m* frames per trigger event are composed to an image with the dimensions of $m \times 1280$ (number of frames × number of channels/pixels).

During this experiment FLASH ran in the multi-bunch mode and generated 80 electron bunches with a bunch frequency of 200 kHz and a train repetition rate of 10 Hz. The 13^{th} electron bunch of every bunch train was kicked out for alignment. As mentioned above, the internal electronics of GOTTHARD control the timing of the pulse exposures after receiving the trigger pulse. The missing pulse helps to find the timing setting for the synchronization of the detection scheme to the pulse train. The GOTTHARD detector was set to take 100 frames with a frequency of 200 kHz and an opening time of 3.3 µs when triggered by the FLASH 10 Hz trigger. The gain was set manually to the highest gain. The resulting average data rate is around some tens of kB/sec for the GMD and the VLS. The GHS generates around 3 MB/s and the PES/PIS experiment around 45 MB/s on average.

III. Results

In the evaluation process the unexposed frames are used to generate an average background signal, which is then subtracted from all frames taken from one pulse train. The composition of the frames one below the other results in images like the one shown exemplarily in figure 3. The first pulse is visible in frame 11 and the last in frame 90. The frames 1 to 10 and 91 to 100 are taken before and after the pulse train, respectively, and just show the noise of the unilluminated sensor. Because the 13^{th} bunch is kicked out, the frame 23 is also empty. The illuminated frames show clearly the photon energy spectra of the 79 light pulses of the pulse train.

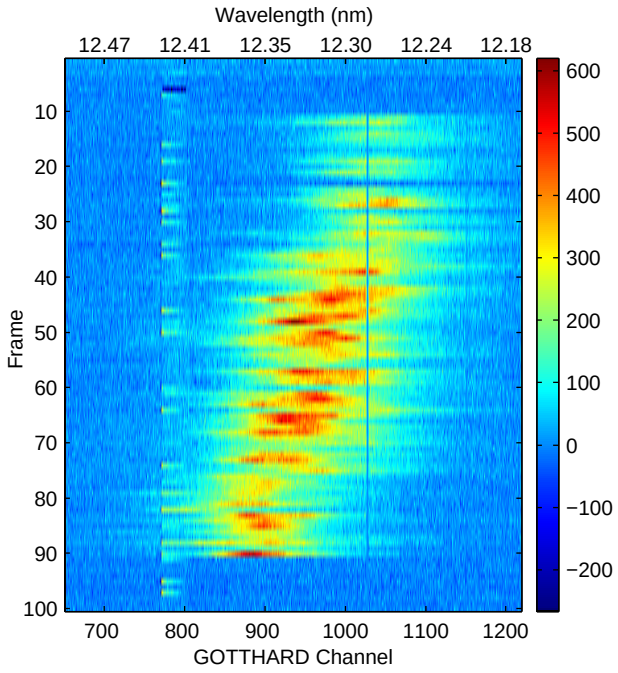

FIG. 3: (Color online) Image of 100 frames taken with a readout frequency of 200 kHz. After some frames without a signal, one can clearly see the wavelength distribution of all pulses of the pulse train and a shift to higher mean wavelengths towards the end of the pulse train. FLASH ran with 200 kHz and 80 bunches (the 13th has been kicked out).

The spectra show the expected SASE related fluctuations of the mean photon energy or wavelength, spectral bandwidth and intensity from pulse to pulse. Furthermore, the mean photon wavelength shows a shift from lower (12.26 nm) to higher (12.36 nm) values from the beginning to the end of the pulse train. This shift is stable over time and depends on FEL machine parameters and settings. Other features are produced by blind pixels around channel 1030 and distortions, which often arise from channel 780 to 800. It is important to mention, that we also successfully recorded pulse spectra with 400 kHz, 600 kHz and 800 kHz readout frequency. Due to current limitation of the internal storage to cache 120 frames in maximum, only a part of the pulse train could be imaged at these higher readout frequencies.

For the purpose as an online tool a similar image as shown in figure 3 can be observed during the measurements in the controlling GUI of the GOTTHARD detector while measuring. The background correction is hereby done by taking few images without light. The software takes these non-illuminated images as background for the correction of the following images.

In figure 4 three different pulses extracted from the pulse train depicted in figure 3 are shown. The spectra are different in shape due to different mode contributions of the FEL. In the spectrum of pulse 75 (red dotted) only one peak is visible, whereas the spectra of the pulses 27 (blue solid) and 53 (green dashed) show a multi-peak structure. Once again one sees the shift in the mean photon wavelength to higher values when going to higher pulse numbers. Except for some deviations originating from spikes, damaged sensor channels or slight variations in the sensor sensitivity due to the etching process the average of all pulses of the pulse train (black thick solid) has a shape of

two to three strongly overlapping Gaussian curves with a total FWHM of 0.12 nm. The structure of multiple Gaussians is a result of the FEL tuning and can be observed over the whole measuring time and also in averaged spectra of the VLS spectrometer.

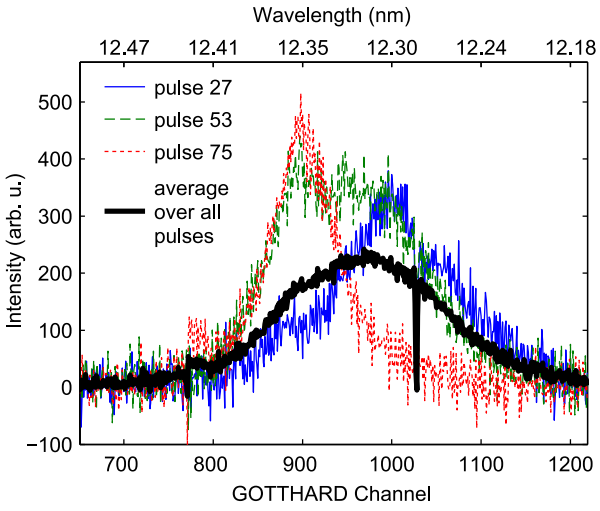

FIG. 4: (Color online) Different single pulse spectra showing the fluctuations in position and shape. The averaged spectrum over the whole train has a shape of two or three strong overlapping Gaussians disturbed by fluctuating or dead pixels of the GOTTHARD detector line.

Note, that the mean count numbers of the pulse maxima are just around 1 % of the saturation limit of the selected gain level. The limiting noise is the 1/f detector noise, especially at the chosen short integration times. The relatively low signal-to-noise ratio results from the strong loss of photons due to the optical elements and the magnification. The FEL pulses entering the chamber get dispersed by the grating whose absolute efficiency can be assumed to be below 1 % in the first order at the used wavelength.[37] The fluorescence of the Ce:YAG is distributed equally in all directions and the first lens covers only a small solid angle of 2.6 %. The strong magnification reduces the flux further and enlarges the fluorescence also in the vertical direction. Due to the single line detection of the GOTTHARD a substantial part of the image hits the housing and is not detected. The number of measured photons can be estimated with the known behavior of the charge integrating amplifier and the number of counts from the mean integrated signal. On average, 10^5 photons per pulse reach the whole sensor area of the detector. Furthermore, GOTTHARD is designed to detect hard x-ray radiation rather than visible, low energy photons.

The GOTTHARD spectrometer is not intrinsically calibrated. To get an energy or wavelength scale, a comparison and correlation to the spectra measured with the VLS spectrometer was used. The calibration procedure is explained by taking the example of the two spectra shown in figure 5.

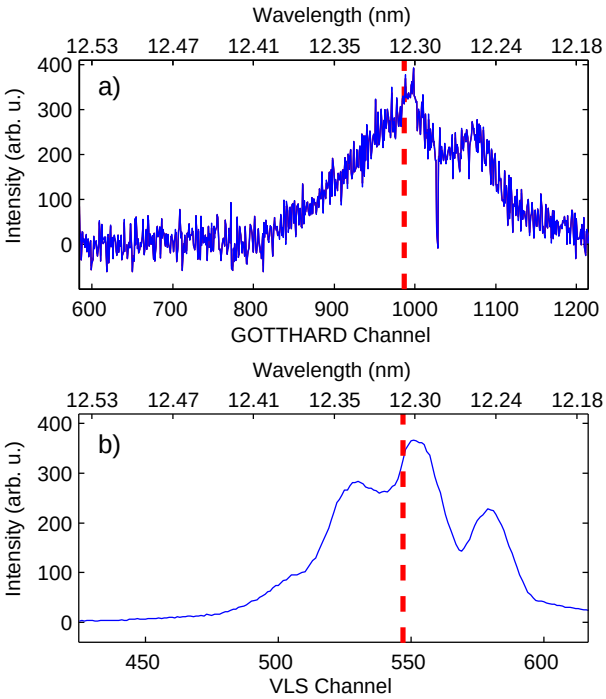

FIG. 5: (Color online) Example of a VLS (a) and a GHS spectrum (b) of the same pulse. The dashed vertical line marks the calculated center of mass (CoM).

The two normalized spectra are taken from the same pulse. The upper spectrum in figure 5(a) is measured with the GOTTHARD spectrometer and the lower one (b) is recorded with the VLS spectrometer. The background correction for the VLS spectra is different from that of the GOTTHARD spectra explained above. The signal far of the flanks of the peak is taken as background baseline and subtracted from the whole spectrum. A calibration function for the VLS spectrometer enables the conversion from channel position into wavelength. The spectrum itself shows a better signal-to-noise ratio compared to the GOTTHARD spectrum due to the use of an intensified CCD. However, both spectra show similar shape apart from the intensity. In the VLS spectrum four peaks can be seen. In the GOTTHARD spectrum the two peaks on the right side are visible, whereas on the left side further peaks are difficult to assign due to the lower signal-to-noise ratio and a slightly lower resolution. The resolution of the GOTTHARD spectrometer is estimated to be about 15 % less compared to the VLS spectrometer. The vertical red dashed line marks the center of mass (CoM). The CoM has been determined for all spectra by integration and searching for the channel which separates the area into two halves. In case of GOTTHARD spectra a smoothing spline is fitted to the data in order to reduce the influence of the noise. During the measurements, the VLS gating has been changed after several minutes of measuring to record spectra from pulses at different position within the pulse trains. The existence and stability of the observed shift in the mean wavelength within the pulse trains are confirmed by the VLS spectra. Their calculated CoMs are used as reference and compared with the CoMs of the corresponding GOTTHARD spectra. In figure 6(a) the CoM of more than 22000 corresponding spectra from both spectrometers are plotted against each other forming a correlation plot.

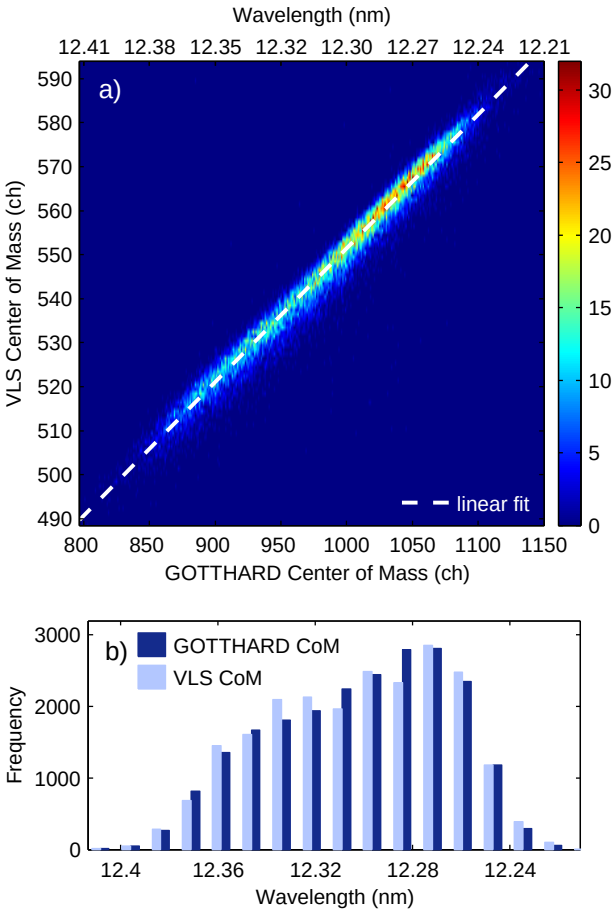

FIG. 6: (Color online) Correlation plot of the center of masses (a) and a histogram of their distribution (b) of more than 22000 corresponding spectra measured with GOTTHARD and the VLS spectrometer. The linear fit to the data (white dashed line) in a) is used for the wavelength calibration of the GOTTHARD spectra.

The plot shows a linear correlation in the observed wavelength window with a correlation coefficient of 0.98. With a linear fit (white dashed line) the wavelength scale from the VLS calibration can be adapted to the GOTTHARD spectra and leads to the wavelength axis of figures 3, 4 and 5. In figure 6(b) a frequency histogram of the CoMs of both spectrometers are plotted, showing similar distributions. The structure showing multiple overlapping Gaussians, already seen in the averaged spectrum of figure 4 and originated in the FEL machine parameters during the measurements, is clearer in the histogram. To estimate the reliability of the CoM values measured with the GOTTHARD spectrometer a statistical analysis has been performed. All CoM values have been normalized to their respective average. Taking the VLS values as reference, the quotient of each GOTTHARD value with its corresponding VLS value is formed. A quotient of 1 would be a perfect correlation. With a histogram of the quotients the deviations of the GOTTHARD CoMs from the ideal correlation within the 1σ, 2σ and the 3σ interval can be determined. The deviations are 3.2 % for 1σ, 5.8 % for the 2σ and 6.6 % for the 3σ interval. The small deviations confirm our findings that the spectrometer with the GOTTHARD detector can be used as a reliable

single-shot analysis tool for the photon energy. Especially, when regarding the intensity and noise sensitive method of defining the CoM, the deviations can be reduced by increasing the signal-to-noise ratio.

Another important issue for the functionality of the new spectrometer is its intensity response. The intensity of FELs is also fluctuating statistically due to the SASE process.[22] A precise knowledge of the intensity or of the number of photons on a shot-to-shot base is vital for most experiments aiming at nonlinear effects in light-matter interaction. For the extraction of the intensity information from the GOTTHARD data, the smoothed spectra have been integrated resulting in pulse intensities in arbitrary units. For a comparison more than 1.7×10^6 values gained by the integration of the GOTTHARD signal are plotted against the corresponding values from the GMD in figure 7. Near zero values arising for example from the data point representing the 13th pulse, whose bunch was kicked out, have been excluded.

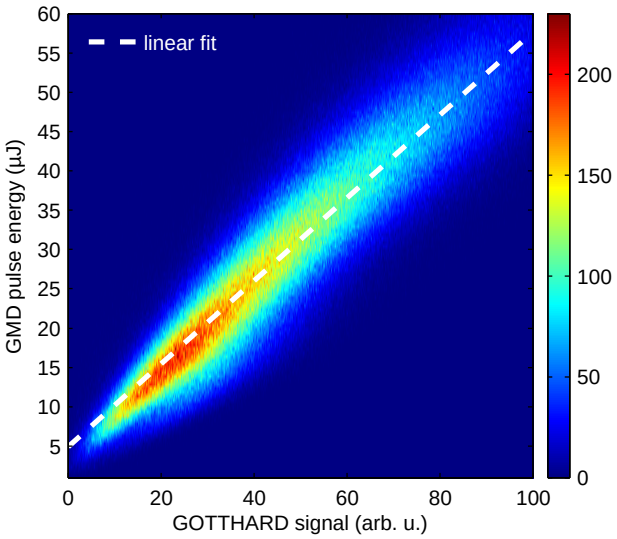

FIG. 7: (Color online) Correlation plot of more than 1.7 million corresponding pulse intensity values. The integrated GOTTHARD signal against the Gas Monitor Detector (GMD) signal is shown and a fitted by a linear function (white dashed line).

A nearly linear correlation can be identified. However, a linear function fitted to the data shows a non-zero y-intercept and clarifies the slight non-linearity. As mentioned above the low photon flux on the detector and the thereof resulting low count rates below 1 % of the saturation limit result in strong influences of distortions and noise. Together with the uncertainty of the GMD values of 10 %[22] this can explain the broad shape of the plot. However, the deviations from linearity and the asymmetrical shape cannot be explained by the signal-to-noise ratio alone. A saturation effect of the GMD is very unlikely at these FEL intensities and a saturation of the crystal would show an inverted curvature than observed. The intensity behavior will be a matter of further investigation and future experiments.

The same statistical analysis done for the CoM dataset above is now applied to the intensity values and the GMD values are taken as reference. The resulting histogram of the quotients of the normalized values is much broader, as

expected. The determined deviations are 21 % in the 1σ, 46 % 2σ and 86 % the 3σ interval. The GMD uncertainty is part of the deviation calculated in the statistical analysis and cannot be assumed as negligible. An increase of the photon flux and the knowledge of the response function in the visible wavelength regime would strongly reduce the uncertainty for the intensity measurement performed with the GOTTHARD detector.

The linear fit extracted from figure 7 is used for a rescaling of the values from the integration of the GOTTHARD spectra for a direct comparison with the GMD signal on a shot-to-shot base. In figure 8 the rescaled intensity values from the pulse train shown in figure 3 are plotted together with their corresponding GMD values.

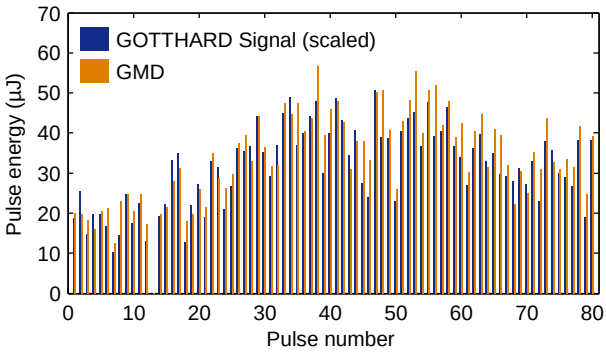

FIG. 8: The scaled integrated signal of the illuminated frames from the GOTTHARD detector compared with the Gas Monitor Detector (GMD) signal of the pulse train shown in figure 3.

One sees the intensity fluctuations from shot to shot within the pulse train. Despite the strong deviations discussed above a good similarity is visible in the behavior between the two datasets. The general trend of the intensity over the pulse train depends on machine parameters and conditions. In our measurement the first approximately twenty pulses were generally lower in intensity.

As a test for the purpose of enhancing the spectral resolution of spectroscopic experiments at FLASH, photo electron spectra of atomic Neon have been obtained in parallel with the PES/PIS chamber. For a reasonable spectrum usually several thousand single shot spectra are averaged. By this nonselective averaging all fluctuations in photon wavelength are also included and result in an additional peak broadening. This broadening is reducible by selecting the photo electron spectra by the CoM of the respective GOTTHARD spectra. In figure 9 the results of two different averaged selections (blue dotted and red dashed) are compared with the unselective average (black solid) of the Ne spectra for the Ne 2p photo emission line. Photoelectron spectra produced by pulses with relatively short mean wavelength from 12.29 nm to 12.32 nm are averaged in the blue dotted spectrum. The red dashed spectrum contains only photo electron spectra which are produced by pulses with relative long mean wavelengths from 12.43 nm to 12.46 nm according to the CoMs of their GOTTHARD spectra.

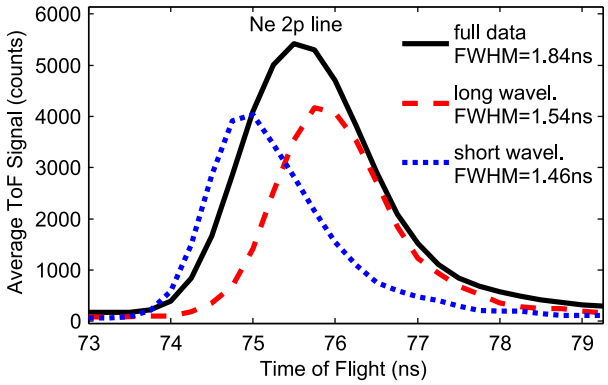

FIG. 9: (Color online) Different averaged Time-of-Flight photoelectron spectra of atomic Neon 2p line taken with the experiment before the GOTTHARD spectrometer. Comparison between unselected data (black solid line), a short wavelength selection containing mean wavelength values from 12.29 nm - 12.32 nm (blue dotted line) and a long wavelength selection containing mean wavelength values from 12.43 nm - 12.46 nm (red dashed line).

As expected, the line of the short wavelength selection has shorter and the long wavelength selection longer flight times than the line containing all data. The selection of single pulse photoelectron spectra with respect to the CoM of corresponding GOTTHARD spectra results in a reduction of the FWHM. Compared to the unselected average of all spectra the selection reduces the FWHM for the Neon 2p line around 17 % for the long wavelength selection and approximately 20 % for the short wavelength selection.

IV. Conclusion and Outlook

We have presented the setup of a new grating spectrometer for the XUV FEL FLASH with the GOTTHARD detector as key element and demonstrated the possibility of measuring photon energy spectra on a shot-to-shot base at FLASH for the first time. Complete pulse trains generated by 80 electron bunches with a bunch repetition rate of 200 kHz were imaged over a long period. Parts of the pulse trains were successfully probed with readout frequencies of up to 800 kHz.

In the obtained photon energy spectra the fluctuations in photon energy and intensity from shot to shot arising from the statistical nature of the SASE process could be clearly observed. In addition, a long term stable shift of the mean photon wavelength to higher values over the pulse train has been found originating in the used machine settings of FLASH. The spectrometer can provide online information on the photon energy as well as the intensity and their progression over the pulse train and can act as an online diagnostic tool for machine studies and tuning.

By using the shot-to-shot wavelength information from the GOTTHARD spectrometer we have demonstrated the ability to enhance the resolution of simultaneously measured photo electron spectra by up to 20 % in this first test. In the future this can boost the experimental value of spectral data at FLASH and later at the European X-FEL.

Therefore, GOTTHARD has met our requirements of a fast, sensitive and reliable detector and was successfully implemented into the FLASH DAQ system. The information gathered during the measurements will boost the development of these kinds of ultrafast detectors and their implementation at various light sources. As an example, different GOTTHARD detector devices are currently under development for the European X-FEL, which will provide readout frequencies of up to 5 MHz, higher frame storage capacity and a more precise clocking.

The next step will be a permanent implementation of the GOTTHARD detector into the VLS spectrometer as an alternative to the currently used ICCD camera. This will open the possibility for shot-to-shot wavelength measurements even for non-transparent experiments. Amplifier, such as micro-channel plates, before the Ce:YAG crystal or another lens geometry can be used to increase the photon flux onto the detector and the signal-to-noise ratio of the measured spectra. With an improved signal-to-noise ratio a full deconvolution of measured photoelectron spectra from the wavelength distribution of the FEL beam will become possible and further enhance the experimental resolution. An additional future possibility is the online measurement of the pulse length, which is a crucial information for time dependent measurements. Using the number of modes in the spectral distribution the pulse length can be estimated via a second order correlation function.[43,44]

V. Acknowledgement

This project was financed by the German Ministry of Education and Research though the Grant No. 05K10HRB within the framework of the priority program: 301-*FLASH: Matter in the light of ultrashort and extremely intense x-ray pulses* and the German Research Foundation (DFG) by the funding No. MA 2561/4-1.

We acknowledge the FLASH team and in particular Günter Brenner for the excellent technical and experimental support during the beamtime and its preparation at FLASH. Furthermore, we thank the FLASH IT division, especially Vladimir Rybnikov, for the implementation of the GOTTHARD device into the FLASH DAQ system and the setup and maintenance of its software and GUI. Stefan Düsterer and Kai Tiedtke from DESY as well as Hendrik Kaser and Alexander Gottwald from the Metrology Light Source of the German National Metrology Institute Berlin deserve our thanks for their help and the opportunity of preparatory measurements and tests. Also, we thank McPherson Inc. for technical support and information regarding the spectrograph.

1 C. Bostedt, H. N. Chapman, J. T. Costello, J. R. C. López-Urrutia, S. Düsterer, S. W. Epp, J. Feldhaus, A. Föhlisch, M. Meyer, T. Möller, R. Moshammer, M. Richter, K. Sokolowski-Tinten, A. Sorokin, K. Tiedtke, J. Ullrich and W. Wurth, Nucl. Instrum. Methods Phys. Res. A **601**, 108-122 (2009).

2 M. Krikunova, T. Maltezopoulos, A. Azima, M. Schlie, U. Frühling, H. Redlin, R. Kalms, S. Cunovic, N. M. Kabachnik, M. Wieland and M. Drescher, New J. Phys. **11**, 123019 (2009).

3 A. A. Sorokin, S. V. Bobashev, T. Feigl, K. Tiedtke, H. Wabnitz and M. Richter, Phys. Rev. Lett. **99**, 213002 (2007).

4 M. Richter, S. V. Bobashev, A. A. Sorokin and K. Tiedtke, J. Phys. Conf. Ser. **141**, 012014 (2008).

5 M. Richter, S.V. Bobashev, A. A. Sorokin and K. Tiedtke, Appl. Phys. A **92**, 473-478 (2008).

6 N. Berrah, J. Bozek, J.T. Costello, S. Düsterer, L. Fang, J. Feldhaus, H. Fukuzawa, M. Hoener, Y.H. Jiang, P. Johnsson, E.T. Kennedy, M. Meyer, R. Moshammer, P. Radcliffe, M. Richter, A. Rouzée, A. Rudenko, A.A. Sorokin, K. Tiedtke, K. Ueda, J. Ullrich and M.J.J. Vrakking, J. Mod. Opt. **57**, 1015-1040 (2010).

7 N. Rohringer and R. Santra, Phys. Rev. A **76**, 033416 (2007).

8 N. Gerken, S. Klumpp, A. A. Sorokin, K. Tiedtke, M. Richter, V. Bürk, K. Mertens, P. Juranić and M. Martins, Phys. Rev. Lett. **112**, 213002 (2014).

9 J. R Schneider, J. Phys. B: At. Mol. Opt. Phys. **43**, 194001 (2010).

10 J. Feldhaus, J. Phys. B: At. Mol. Opt. Phys. **43**, 194002 (2010).

11 K. Tiedtke, A. Azima, N. von Bargen, L. Bittner, S. Bonfigt, S. Düsterer, B. Faatz, U. Frühling, M. Gensch, Ch. Gerth, N. Guerassimova, U. Hahn, T. Hans, M. Hesse, K. Honkavaar, U. Jastrow, P. Juranic, S. Kapitzki, B. Keitel, T. Kracht, M. Kuhlmann, W. B. Li, M. Martins, T. Núñez, E. Plönjes, H. Redlin, E. L. Saldin, E. A. Schneidmiller, J. R. Schneider, S. Schreiber, N. Stojanovic, F. Tavella, S. Toleikis, R. Treusch, H. Weigelt, M. Wellhöfer, H. Wabnitz, M. V. Yurkov and J. Feldhaus, New J. Phys. **11**, 023029 (2009).

12 W. Ackermann, G. Asova, V. Ayvazyan, A. Azima, N. Baboi, J. Bähr, V. Balandin, B. Beutner, A. Brandt, A. Bolzmann, R. Brinkmann, Brovko, O. I., M. Castellano, P. Castro, L. Catani, E. Chiadroni, S. Choroba, A. Cianchi, Costello, J. T., D. Cubaynes, J. Dardis, W. Decking, H. Delsim-Hashemi, A. Delserieys, G., Di Pirro, M. Dohlus, S. Düsterer, A. Eckhardt, Edwards, H. T., B. Faatz, J. Feldhaus, K. Flöttmann, J. Frisch, L. Fröhlich, T. Garvey, U. Gensch, Ch. Gerth, M. Görler, N. Golubeva, H.-J. Grabosch, M. Grecki, O. Grimm, K. Hacker, U. Hahn, Han, J. H., K. Honkavaara, T. Hott, M. Hüning, Y. Ivanisenko, E. Jaeschke, W. Jalmuzna, T. Jezynski, R. Kammering, V. Katalev, K. Kavanagh, Kennedy, E. T., S. Khodyachykh, K. Klose, V. Kocharyan, M. Körfer, M. Kollewe, W. Koprek, S. Korepanov, D. Kostin, M. Krassilnikov, G. Kube, M. Kuhlmann, Lewis, C. L. S., L. Lilje, T. Limberg, D. Lipka, F. Löhl, H. Luna, M. Luong, M. Martins, M. Meyer, P. Michelato, V. Miltchev, Möller, W. D., L. Monaco, Müller, W. F. O., O. Napieralski, O. Napoly, P. Nicolosi, D. Nölle, T. Nunez, A. Oppelt, C. Pagani, R. Paparella, N. Pchalek, J. Pedregosa-Gutierrez, B. Petersen, B. Petrosyan, G. Petrosyan, L. Petrosyan, J. Pflüger, E. Plönjes, L. Poletto, K. Pozniak, E. Prat, D. Proch, P. Pucyk, P. Radcliffe, H. Redlin, K. Rehlich, M. Richter, M. Roehrs, J. Roensch, R. Romaniuk, M. Ross, J. Rossbach, V. Rybnikov, M. Sachwitz, Saldin, E. L., W. Sandner, H. Schlarb, B. Schmidt, M. Schmitz, P. Schmüser, Schneider, J. R., Schneidmiller, E. A., S. Schnepp, S. Schreiber, M. Seidel, D. Sertore, Shabunov, A. V., C. Simon, S. Simrock, E. Sombrowski, Sorokin, A. A., P. Spanknebel, R. Spesyvtsev, L. Staykov, B. Steffen, F. Stephan, F. Stulle, H. Thom, K. Tiedtke, M. Tischer, S. Toleikis, R. Treusch, D. Trines, I. Tsakov, E. Vogel, T. Weiland, H. Weise, M. Wellhöfer, M. Wendt, I. Will, A. Winter, K. Wittenburg, W. Wurth, P. Yeates, Yurkov, M. V., ZagorodnovI. and K. Zapfe, Nat. Photonics **1**, 336-342 (2007).

13 V. Ayvazyan, N. Baboi, J. Bähr, V. Balandin, B. Beutner, A. Brandt, I. Bohnet, A. Bolzmann, R. Brinkmann, O. I. Brovko, J. P. Carneiro, S. Casalbuoni, M. Castellano, P. Castro, L. Catani, E. Chiadroni, S. Choroba, A. Cianchi, H. Delsim-Hashemi, G. Di Pirro, M. Dohlus, S. Düsterer, H. T. Edwards, B. Faatz, A. A. Fateev, J. Feldhaus, K. Flöttmann, J. Frisch, L. Fröhlich, T. Garvey, U. Gensch, N. Golubeva, H.-J. Grabosch, B. Grigoryan, O. Grimm, U. Hahn, J. H. Han, M. V. Hartrott, K. Honkavaara, M. Hüning, R. Ischebeck, E. Jaeschke, M. Jablonka, R. Kammering, V. Katalev, B. Keitel, S. Khodyachykh, Y. Kim, V. Kocharyan, M. Körfer, M. Kollewe, D. Kostin, D. Krämer, M. Krassilnikov, G. Kube, L. Lilje, T. Limberg, D. Lipka, F. Löhl, M. Luong, C. Magne, J. Menzel, P. Michelato, V. Miltchev, M. Minty, W. D. Möller, L. Monaco, W. Müller, M. Nagl, O. Napoly, P. Nicolosi, D. Nölle, T. Nunez, A. Oppelt, C. Pagani, R. Paparella, B. Petersen, B. Petrosyan, J. Pflüger, P. Piot, E. Plönjes, L. Poletto, D. Proch, D. Pugachov, K. Rehlich, D. Richter, S. Riemann, M. Ross, J. Rossbach, M. Sachwitz, E. L. Saldin, W. Sandner, H. Schlarb, B. Schmidt, M. Schmitz, P. Schmüser, J. R. Schneider, E. A. Schneidmiller, H.-J. Schreiber, S. Schreiber, A. V. Shabunov, D. Sertore, S. Setzer, S. Simrock, E. Sombrowski, L. Staykov, B. Steffen, F. Stephan, F. Stulle, K. P. Sytchev, H. Thom, K. Tiedtke, M. Tischer, R. Treusch, D. Trines, I. Tsakov, A. Vardanyan, R. Wanzenberg, T. Weiland, H. Weise, M. Wendt, I. Will,

A. Winter, K. Wittenburg, M. V. Yurkov, I. Zagorodnov, P. Zambolin and K. Zapfe, Eur. Phys. J. D **37**, 297-303 (2006).

14 S. Düsterer, M. Rehders, A. Al-Shemmary, C. Behrens, G. Brenner, O. Brovko, M. DellAngela, M. Drescher, B. Faatz, J. Feldhaus, U. Frühling, N. Gerasimova, N. Gerken, C. Gerth, T. Golz, A. Grebentsov, E. Hass, K. Honkavaara, V. Kocharian, M. Kurka, Th. Limberg, R. Mitzner, R. Moshammer, E. Plönjes, M. Richter, J. Rönsch-Schulenburg, A. Rudenko, H. Schlarb, B. Schmidt, A. Senftleben, E. A. Schneidmiller, B. Siemer, F. Sorgenfrei, A. A. Sorokin, N. Stojanovic, K. Tiedtke, R. Treusch, M. Vogt, M. Wieland, W. Wurth, S. Wesch, M. Yan, M. V. Yurkov, H. Zacharias and S. Schreiber, Phys. Rev. ST Accel. Beams **17**, 120702 (2014).

15 M. Altarelli, Technical Design Report Report No. ISBN 978-3-935702-17-1, 2006.

16 A. M. Kondratenko and E. L. Saldin, Sov. Phys. Dokl. **24**, 986 (1979).

17 A. M. Kondratenko and E. L. Saldin, Part. Accel. **10**, 207-216 (1980).

18 R. Bonifacio, C. Pellegrini and L.M. Narducci, Opt. Commun. **50**, 373-378 (1984).

19 P. Emma, R. Akre, J. Arthur, R. Bionta, C. Bostedt, J. Bozek, A. Brachmann, P. Bucksbaum, R. Coffee, F.-J. Decker, Y. Ding, D. Dowell, S. Edstrom, A. Fisher, J. Frisch, S. Gilevich, J. Hastings, G. Hays, Ph. Hering, Z. Huang, R. Iverson, H. Loos, M. Messerschmidt, A. Miahnahri, S. Moeller, H.-D. Nuhn, G. Pile, D. Ratner, J. Rzepiela, D. Schultz, T. Smith, P. Stefan, H. Tompkins, J. Turner, J. Welch, W. White, J. Wu, G. Yocky and J. Galayda, Nat Photon **4**, 641-647 (2010).

20 E.L. Saldin, E.A. Schneidmiller and M.V. Yurkov, Nucl. Instrum. Methods Phys. Res. A **507**, 101-105 (2003).

21 V. Ayvazyan, J.-P. Carneiro, P. Castro, B. Faatz, A. A. Fateev, J. Feldhaus, Ch. Gerth, V. Gretchko, B. Grigoryan, U. Hahn, K. Honkavaara, M. Hüning, R. Ischebeck, U. Jastrow, R. Kammering, J. Menzel, M. Minty, D. Nölle, J. Pflüger, Ph. Piot, L. Plucinski, K. Rehlich, J. Rossbach, E. L. Saldin, H. Schlarb, E. A. Schneidmiller, S. Schreiber, R. Sobierajski, B. Steeg, F. Stulle, K. P. Sytchev, K. Tiedtke, R. Treusch, H. Weise, M. Wendt and M. V. Yurkov, Nucl. Instrum. Methods Phys. Res. A **507**, 368-372 (2003).

22 K. Tiedtke, J. Feldhaus, U. Hahn, U. Jastrow, T. Nunez, T. Tschentscher, S. V. Bobashev, A. A. Sorokin, J. B. Hastings, S. Möller, L. Cibik, A. Gottwald, A. Hoehl, U. Kroth, M. Krumrey, H. Schöppe, G. Ulm and M. Richter, J. Appl. Phys. **103**, 094511 (2008).

23 R. Riedel, A. Al-Shemmary, M. Gensch, T. Golz, M. Harmand, N. Medvedev, M. J. Prandolini, K. Sokolowski-Tinten, S. Toleikis, U. Wegner, B. Ziaja, N. Stojanovic and F. Tavella, Nat. Commun. **4**, 1731 (2013).

24 V. Senz, T. Fischer, P. Oelßner, J. Tiggesbäumker, J. Stanzel, C. Bostedt, H. Thomas, M. Schöffler, L. Foucar, M. Martins, J. Neville, M. Neeb, Th. Möller, W. Wurth, E. Rühl, R. Dörner, H. Schmidt-Böcking, W. Eberhardt, G. Ganteför, R. Treusch, P. Radcliffe and K.-H. Meiwes-Broer, Phys. Rev. Lett. **102**, 138303 (2009).

25 J. Bahn, P. Oelßner, M. Köther, C. Braun, V. Senz, S. Palutke, M. Martins, E. Rühl, G. Ganteför, T. Möller, B. von Issendorff, D. Bauer, J. Tiggesbäumker and K.-H. Meiwes-Broer, New J. Phys. **14**, 075008 (2012).

26 M. Martins, M. Wellhöfer, J. T. Hoeft, W. Wurth, J. Feldhaus and R. Follath, Rev. Sci. Instrum. **77**, 115108 (2006).

27 M. Martins, M. Wellhöfer, A. A. Sorokin, M. Richter, K. Tiedtke and W. Wurth, Phys. Rev. A **80**, 023411 (2009).

28 F. Frassetto, S. Coraggia, N. Gerasimova, S. Dziarzhytski, T. Golz, H. Weigelt and L. Poletto, Nucl. Instrum. Methods Phys. Res. A **635**, S94 - S98 (2011).

29 B. Henrich, J. Becker, R. Dinapoli, P. Goettlicher, H. Graafsma, H. Hirsemann, R. Klanner, H. Krueger, R. Mazzocco, A. Mozzanica, H. Perrey, G. Potdevin, B. Schmitt, X. Shi, A.K. Srivastava, U. Trunk and C. Youngman, Nucl. Instrum. Methods Phys. Res. A **633, Supplement 1**, S11 - S14 (2011).

30 A. Mozzanica, A. Bergamaschi, R. Dinapoli, H. Graafsma, B. Henrich, P. Kraft, I. Johnson, M. Lohmann, B. Schmitt and X. Shi, Nucl. Instrum. Methods Phys. Res. A **633, Supplement 1**, S29 - S32 (2011).

31 A. Mozzanica, A. Bergamaschi, R. Dinapoli, H. Graafsma, D. Greiffenberg, B. Henrich, I. Johnson, M. Lohmann, R. Valeria, B. Schmitt and S. Xintian, J. Instrum. **7**, C01019 (2012).

32 M. Wellhöfer, J. T. Hoeft, M. Martins, W. Wurth, M. Braune, J. Viefhaus, K. Tiedtke and M. Richter, J. Instrum. **3**, P02003 (2008).

33 P. N. Juranic, M. Martins, J. Viefhaus, S. Bonfigt, L. Jahn, M. Ilchen, S. Klumpp and K. Tiedtke, J. Instrum. **4**, P09011 (2009).

34 D. Greiffenberg, J. Instrum. **7**, C01103 (2012).

35 M. Koike, T. Namioka, E. M. Gullikson, Y. Harada, S. Ishikawa, T. Imazono, S. Mrowka, N. Miyata, M. Yanagihara, J. H. Underwood, K. Sano, T. Ogiwara, O. Yoda and S. Nagai, Proc. SPIE **4146**, 163-170 (2000).

36 T. Yamazaki, E. Gullikson, N. Miyata, M. Koike, Y. Harada, S. Mrowka, U. Kleineberg, J. H. Underwood, M. M. Yanagihara and K. Sano, Appl. Opt. **38**, 4001-4003 (1999).

37 M. Koike, K. Sano, E.c Gullikson, Y. Harada and H. Kumata, Rev. Sci. Instrum. **74**, 1156-1158 (2003).

38 M. B. Chowdhuri, S. Morita, M. Goto, H. Nishimura, K. Nagai and S. Fujioka, Rev. Sci. Instrum. **78**, 023501 (2007).

39 M. Wellhöfer, M. Martins, W. Wurth, A. A. Sorokin and M. Richter, Journal of Optics A: Pure and Applied Optics **9**, 749 (2007).

40 G. Brenner, S. Kapitzki, M. Kuhlmann, E. Ploenjes, T. Noll, F. Siewert, R. Treusch, K. Tiedtke, R. Reininger, M.D. Roper, M.A. Bowler, F.M. Quinn and J. Feldhaus, Nucl. Instrum. Methods Phys. Res. A **635**, S99-S103 (2011).

41 M. Richter, A. Gottwald, U. Kroth, A. A. Sorokin, S. V. Bobashev, L. A. Shmaenok, J. Feldhaus, Ch. Gerth, B. Steeg, K. Tiedtke and R. Treusch, Appl. Phys. Lett. **83**, 2970-2972 (2003).

42 N. C. Gerken, Ph.D. dissertation,University of Hamburg ,2014.

43 E.L. Saldin, E.A. Schneidmiller and M.V. Yurkov, Opt. Commun. **148**, 383-403 (1998).

44 A. A. Lutman, Y. Ding, Y. Feng, Z. Huang, M. Messerschmidt, J. Wu and J. Krzywinski, Phys. Rev. ST Accel. Beams **15**, 030705 (2012).